JOURNAL OF GEOPHYSICAL RESEARCH, VOL. 90, NO. B13, PAGES 11,355–11,366, NOVEMBER 10, 1985

Planar High-Angle Faulting in the Basin and Range: Geodetic Analysis of the 1983 Borah Peak, Idaho, Earthquake

ROSS S. STEIN

U.S. Geological Survey, Menlo Park, California

SERGIO E. BARRIENTOS

C. F. Richter Laboratory, University of California, Santa Cruz

Geodetic elevation changes record the broad-scale deformation associated with the M = 7.0 October 28, 1983, Borah Peak, Idaho, earthquake on the Lost River fault. The crest of the Lost River Range rose 0.2 m, and adjacent Thousand Springs Valley subsided 1.0 m, in relation to reference points 45 km from the main shock epicenter. The deformation was modeled by dislocations in an elastic half-space. A planar fault with uniform dip slip of 2.05 ± 0.10 m, dipping $47° \pm 2°$SW and extending to a vertical depth of 13.3 ± 1.2 km, fits the geodetic data best and is also consistent with the main shock hypocenter and fault plane solution. The geodetic moment is $2.6 \pm 0.5 \times 10^{19}$ N m ($2.6 \pm 0.5 \times 10^{26}$ dyn cm), and the estimated static stress drop is 2.9 ± 0.4 MPa (29 ± 4 bars). Tests for coseismic slip on listric faults (which flatten with depth) and on detachments (horizontal faults or shear zones) showed fits to the geodetic data that are inferior to those for planar high-angle faults. No detectable coseismic slip occurred on the Mesozoic White Knob thrust fault, although the low-angle thrust sheet intersects the south end of Lost River fault near the 1983 mainshock epicenter. If the high-angle Lost River fault abuts a flat-lying detachment fault or shear zone, such a structure must lie at depths of >12 km, near the brittle-ductile transition, where stick-slip behavior gives way to creep. The depth and geometry of faulting at Borah Peak is similar to that inferred from seismic and geodetic evidence for the 1954 M = 7.2 Fairview Peak, Nevada, and the 1959 M = 7.3 Hebgen Lake, Montana, events, suggesting that if detachments are active at these localities, they are deep and most likely slip by creep.

INTRODUCTION

Today, more than a century after *LeConte* [1878] and *Gilbert* [1884] first studied the earthquake potential of the Basin and Range province following the M = 7.8 1872 Owens Valley, California, earthquake, we still depend on large earthquakes and the permanent deformation they produce at the surface to investigate the mechanics of faulting. Six large historical earthquakes (M > 7) have struck the Great Basin (Table 1); of these, only the 1954 M = 7.2 Fairview Peak, Nevada, the 1959 M = 7.3 Hebgen Lake, Montana, and the 1983 M = 7.0 Borah Peak, Idaho, shocks have left a seismic and geodetic record that enables study of the subsurface fault slip (moment magnitudes cited; see *Hanks and Kanamori* [1979]. From this limited sample and from geologic observations, we must assess seismic hazards in the seven western states shown in Figure 1. The damage that can be inflicted by large earthquakes in this region depends, first, on the proximity of the active faults to population centers and, second, on the subsurface geometry of these faults.

Whether active faults in the Basin and Range province commonly become listric (decrease in dip to become flat lying) or dip steeply at depth is not known. Resolution of this question is crucial not only to evaluate earthquake hazards but also to understand the mechanism and amount of extension across the Great Basin. Rupture of listric and detachment (flat-lying) faults suggests a shallower seismic source (3–10 km) that can locate farther from the fault trace than does rupture at the base of the seismogenic crust (15 km deep) on planar high-angle faults.

Estimates of total extension across the 750-km-wide Great Basin range from 10% [*Stewart*, 1971] to 100% [*Hamilton*, 1985]. The range-bounding normal faults within the Great Basin dip 45°–70° at the surface, but planar faults with these dips cannot accommodate more than about 25% extension unless the faults are rooted to horizontal slip surfaces or ductile shear zones [*Davis*, 1980]. Mesozoic thrust sheets may underly many of the high-angle faults, however, supplying the requisite horizontal slip surfaces. Reactivation of the midcrustal thrust sheets as sites of normal slippage requires greatly elevated pore pressures, which have yet to be measured in situ. Great extension may also be accommodated by ductile shear. Ductile shear zones should lie below the depth of peak crustal strength, which occurs at approximately 10–15 km [*Sibson*, 1982]. Recently, geological mapping and deep seismic reflection profiling in the Great Basin [e.g., *Wernicke*, 1981; *Allmendinger et al.*, 1983; *Crone and Harding*, 1984; *Smith and Bruhn*, 1984] and teleseismic waveform modeling in other regions of continental extension [*Eyidoğan and Jackson*, 1985] have been offered as new support for listric faults that merge into detachments and shear zones in the upper crust (3–10 km), a geometry first proposed by *Longwell* [1945].

The 1983 Borah Peak earthquake affords a rare opportunity to delineate the subsurface fault geometry of an active normal fault, particularly since none of the listric or horizontal reflectors identified as faults have been observed to slip seismically. We use the geodetic record of the Borah Peak earthquake to distinguish between planar and listric fault slip and to identify the maximum depth of seismic slip. We find that high-angle faulting extended to the base of the seismogenic crust and was accompanied by no detectable detachment slip. We also compare the coseismic model with the earthquake source parameters measured from seismic radiation at much shorter periods than the geodetic observations and find these measurements to be compatible. Finally, we compare the

Paper number 5B5439.
0148-0227/85/005B-5439$05.00

TABLE 1. Large Historical Basin and Range Earthquakes

Date	Location	Moment Magnitude M	Reference
Jan. 9, 1872	Owens Valley, California	7.8	*Hanks and Kanamori* [1979]
Oct. 2, 1915	Pleasant Valley, Nevada	7.2	*Wallace* [1984*b*]
Dec. 10, 1932	Cedar Mountain, Nevada	7.0	*Doser* [1985*a*]
Dec. 16, 1954	Fairview Peak, Nevada	7.2	*Doser* [1985*a*]
Aug. 19, 1959	Hebgen Lake, Montana	7.3	*Doser* [1985*a*]
Oct. 28, 1983	Borah Peak, Idaho	7.0	*Doser* [1985*a*]; this paper

coseismic deformation with the cumulative deformation preserved in the geologic structure.

Geodetic Data

The precision and spatial coverage of the geodetic data equal or surpass all records of vertical elevation changes associated with large normal faulting earthquakes. The 70-km-long first- and second-order leveling route that crosses the Lost River fault permits estimation of the fault geometry and slip independent of the seismic and geological data.

The coseismic elevation changes were obtained by subtracting the relative heights of bench marks (BM's) surveyed after the earthquake in July 1984 from the heights of the same BM's surveyed before the earthquake in 1933 and 1948 (Figure 2*a*). The top panel of Figure 3 shows the profile of coseismic elevation change, projected onto an azimuth normal to the Lost River fault. Note that what we refer to as the "coseismic period" includes the 50 years preceding the earthquake and the 8 months after it, under the assumption that no artificial subsidence and no preearthquake deformation took place during this period. Tests of this assumption are discussed in the next section. All leveling was conducted by the National Geodetic Survey (NGS); the 1984 survey was carried out at the request of the U.S. Geological Survey (USGS).

In spirit leveling, height differences are measured between adjacent BM's by sighting a horizontal telescope on graduated

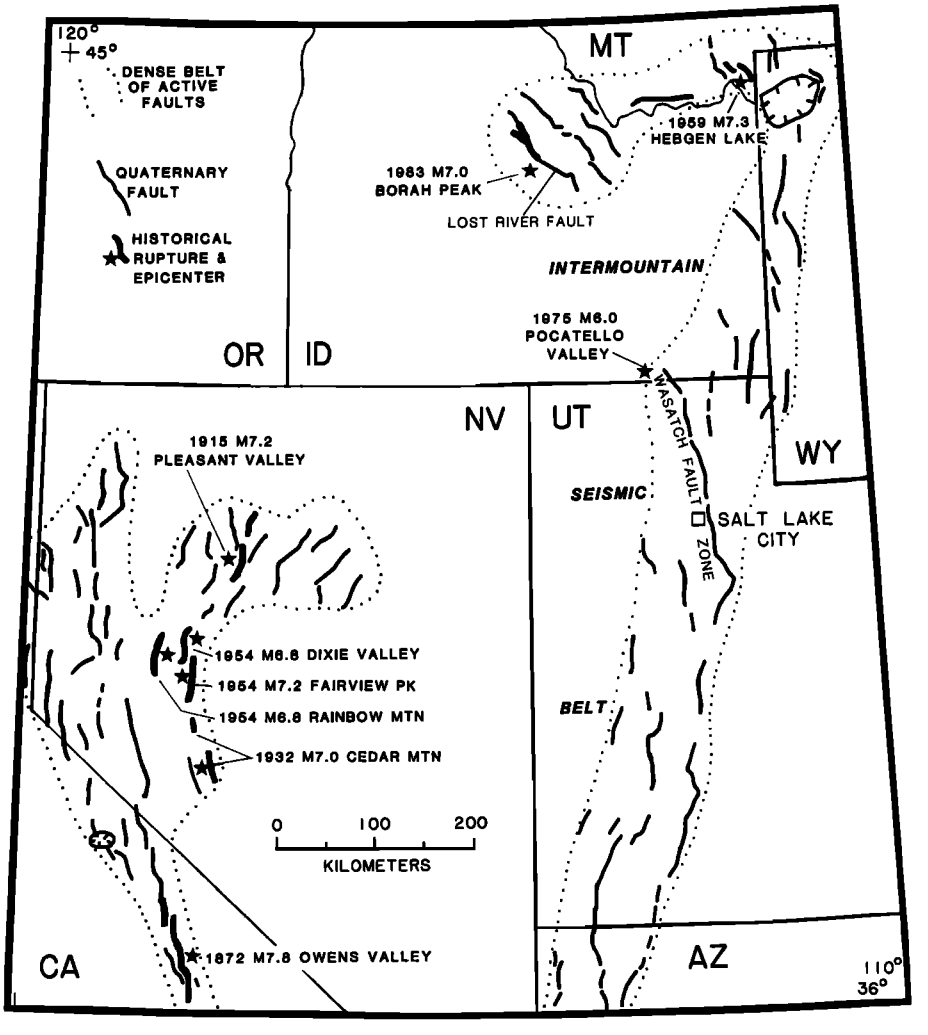

Fig. 1. Sketch of Basin and Range province of the western United States, after *Nakata et al.* [1982], *Wallace* [1984*a*, *b*], and *Scott et al.* [1985], showing locations of earthquakes discussed in text.

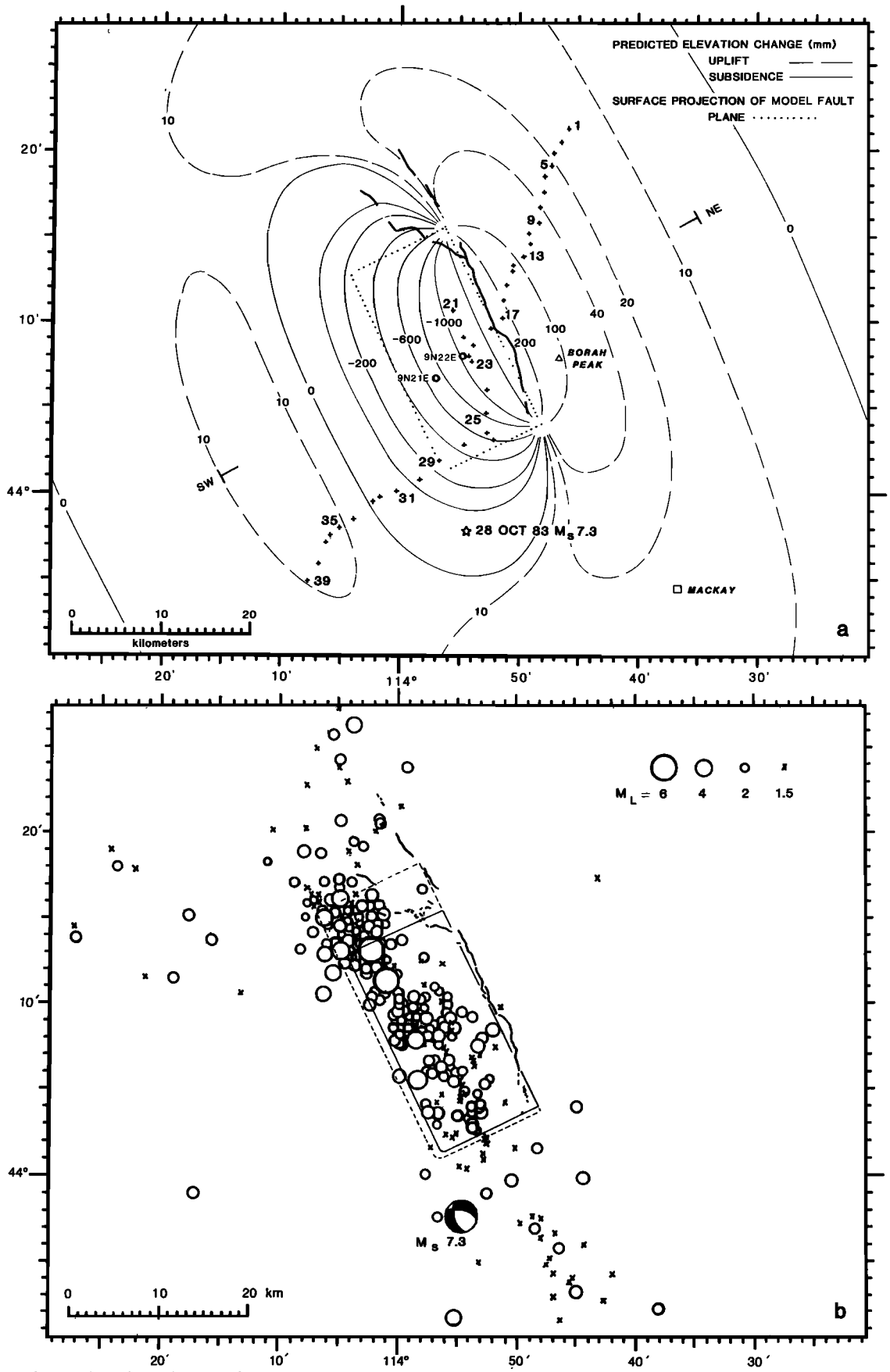

Fig. 2. (*a*) Schematic map of Borah Peak earthquake site, showing locations of epicenter from *Richins et al.* [1985], surface rupture from *Crone and Machette* [1984], and BM's (crosses); contours of elevation change predicted by the coseismic model (dotted rectangle with rounded corners representing the base of the fault); and the line of projection for the profiles in Figures 3, 4, and 6. (*b*) Map showing surface rupture and locations of the October 28, 1983, main shock and aftershocks from October 29 to November 19, 1983 [*Richins et al.*, 1985], coseismic fault model. The solid rectangle is the surface projection of the fault plane; the dashed rectangle is the largest fault plane compatible with the observations, representing a 10% increase in model residuals over the best fit.

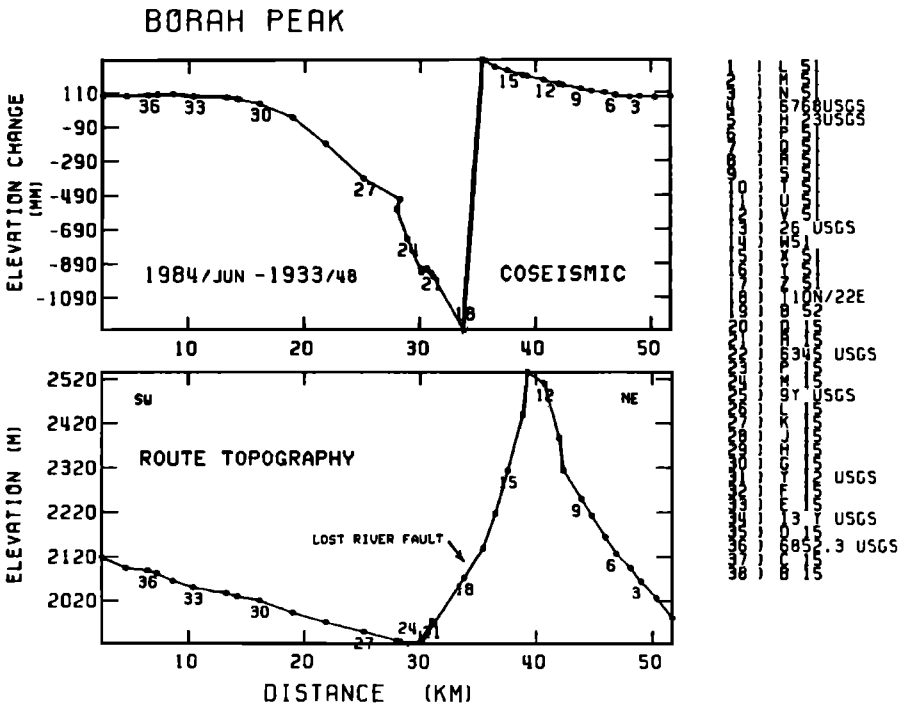

Fig. 3. (Top) Profile of coseismic elevation change projected normal to the fault. (Bottom) Leveling route topography.

rods. All data were corrected for level collimation (horizontal plumb of the level telescope), rod excess (calibration of rod graduations), rod thermal expansion (rod length change as a function of temperature), and atmospheric refraction (bending of the line of sight through vertically stratified air). The observed rod temperatures were used for all surveys to compute rod expansion. For the 1933 and 1948 surveys the thermal coefficient of expansion was assumed; for the 1984 survey it was measured at the National Bureau of Standards. The 1933 and 1948 surveys were corrected for refraction by using the REDUC4 program of *Holdahl* [1981], in which temperature gradients are modeled as a function of time and location, whereas the 1984 observations were corrected following *Kukkamaki* [1938], using observed temperature differences made at every instrument setup.

Survey Errors

Potential sources of noise in the data include random and systematic surveying errors and nontectonic subsidence due to groundwater withdrawal. Estimated cumulative random error for the observed elevation changes nowhere exceeds 20 mm. Briefly, BM's are spaced 1–2 km apart (a pair of adjacent BM's is called a section). The elevation difference over each section can be obtained once or twice during a survey, by surveying forward and backward. If double run, the section is rejected and rerun if the two levelings do not agree within the prescribed section tolerance. The mean differences for all (forward-backward) runnings must not differ significantly from zero, and the standard deviation of the difference, β, gives a good indication of the random error per section. The random error σ should propagate with the square root of the distance leveled: $\sigma = \alpha L^{1/2}$, where σ is in millimeters, α is a function of β, and L is the distance in kilometers [*Bomford*, 1971]. In principle, if β is Gaussian distributed and the survey is double run with BM's spaced 1 km apart, α should be about one third of β. Because some of the 1984 survey was single run using the procedure of *Whalen and Balazs* [1977], we set $\alpha = \beta$ (Table 2 lists the values for α and β). Thus the cumulative random error for the 70-km-long postearthquake survey is 1.38 mm ($L^{1/2}$) = 12 mm. For the 1933 survey, $\beta = 1.83$ mm, slightly larger than β for 1983 or 1984. Because the 1948 leveling segment was single run, β cannot be accurately assessed. We assume here that a value of $\alpha = 2.0$ mm provides a fair estimate for the combined 1933 and 1948 surveys; the cumulative error for the preearthquake leveling is then 17 mm. The random error for elevation change differenced from the preearthquake and postearthquake surveys becomes $(\alpha_1^2 + \alpha_2^2)^{1/2} L^{1/2}$, where the subscript 1 denotes 1984 and the subscript 2 denotes

TABLE 2. Leveling Specifications

NGS Line	Survey Period	Segment, Start BM–End BM	Double or Single Run	Order of Leveling	Reruns, %	Rejection Tolerance, mm	β, mm
L24832	June 19–July 12, 1984	6345 USGS–E15	single	first	4.7	4.0	1.38
		L51–6345; E15–B15	double	first	6.8	4.0	
L24812	Nov. 14–23, 1983	Y51–E15	double	first	1.2	4.0	1.09
L12785	Aug. 18–23, 1948	L51–P15	single	second	4.0	8.4	···
L951	Oct. 4–Nov. 24, 1933	6345 USGS–B15	double	first	4.8	4.0	1.83

Indices are explained in the text and by *Federal Geodetic Control Committee* [1984].

1933/1948. The cumulative or maximum expected error is 20 mm, about the size of the dots in Figure 3, and only about 1% of the maximum coseismic signal. Table 2 lists the leveling specifications.

We examine all surveys for elevation-dependent error, using the method of *Stein* [1981], and found none. Inaccurate rod calibration corrections and, under some circumstances, unmodeled refraction error cause a dependence of elevation change on the elevation. In these cases, elevation change and elevation profiles tend to mimic or mirror each other and thus disclose a systematic error unaccounted for by random error estimates. If tilt and slope were correlated, this error could be identified and removed. Regression coefficients were calculated, but the fact that none of these coefficients departs significantly from zero indicates no systematic errors larger than the limits of detection, 20 ppm times the maximum topographic height difference (600 m), or 12 mm. *Stein and Barrientos* [1985] plot tilt as a function of slope for this data and give the detailed statistics. Although tilt and slope can be related tectonically, *McTigue and Stein* [1984] showed that topographic amplification of stress produces elevation-dependent correlations of only a few parts per million. Because the end points of the coseismic survey lie at nearly the same elevation, these BM's are essentially unaffected by slope-dependent errors. Two isolated BM's that showed elevation changes about 400 mm larger than adjacent BM's were eliminated from the model fitting as unstable.

Subsidence Errors

Hydrologic data demonstrate near stasis of the water table during the coseismic period (1933–1984), making subsidence due to fluid withdrawal unlikely. A reconnaissance water resource survey of the valley [*Stearns et al.*, 1938, Plate 31] indicates that the water stood 3–6 m below the ground surface in 1930–1937 in the vicinity of BM 6345 USGS (BM 22, Figure 2*a*). USGS observation well 9N22E-06CCA1, which was drilled about 150 m west of BM 22 (6345 USGS) in 1967, was observed in 1967–1968, 1978, and 1983–1984 (see Figure 2*a*). The water table stayed 5.4 ± 0.9 m below the surface during 1967–1984, indistinguishable from the 1930–1937 level obtained by reconnaissance. USGS observation well 9N21E-14BBC1, located 4 km west of P15 (BM 23, Figure 2*a*), provides a continuous hydrograph during 1966–1984. This well also shows a constant hydraulic head with only 1-m seasonal fluctuations (see the record of *Whitehead et al.* [1984]). The water table remained static because the alluvial aquifer beneath the leveling route has been recharged by canal diversions from the Big Lost River since 1931 [*Crosthwaite et al.*, 1970].

The 1933 leveling (BM's 1–23) and the 1948 leveling (BM's 22–38) overlap one section at BM's 22–23 (6345 USGS–P15). We used the junction section to test for tilt during 1933–1948. The 1933 and 1948 measurements of height difference over the junction section differ by only 1.56 mm, less than the expected random error for either survey. The absence of measurable tilt during this 15-year period in Thousand Springs Valley supplies a weak test of our assumption that deformation or subsidence preceding the earthquake was negligible.

To summarize, the cumulative uncertainty of BM displacements at each end of the leveling route is 20 mm; the uncertainty of points of greatest relief (km 30–km 40, Figure 3) is nearly the same, owing to smaller random error and a larger potential for slope-dependent error. The uncertainty in elevation change of adjacent BM's is less than 2 mm.

ANALYSIS

Coseismic Model

We seek the simplest dislocation that can explain the observed elevation changes, subject to surveying errors. Fault slip is approximated by uniform displacement on rectangular surfaces embedded in an elastic half-space, using the expressions of *Mansinha and Smylie* [1971]. We neglect the effect of surface topography [*McTigue and Segall*, 1984], changes in elastic moduli with depth, and the stress singularities at the perimeter of the model fault plane.

Our strategy was, first, to model a fault of infinite length along strike. We found the fault dip and width (downdip dimension) that gives the best fit to the data, solving for the absolute elevation change (or zero datum) and the fault slip by minimizing residuals in a least squares sense. We then model a fault with finite length, striking parallel to the surface rupture, using the two-dimensional results as a guide. By trial and error we find the dip, width, and fault length that minimize the residuals. Faults with only pure dip slip were modeled because a lateral slip component of $\pm 10°$ (up to 17% of the dip slip) cannot be discriminated without BM's at both fault ends. We made no attempt to make the model fault consistent with the main shock hypocenter, its fault plane solution, or the locations of aftershocks. Although the distribution of BM's does not permit accurate location of the north fault end, quite high sensitivity to the termination of slip at the south end of the fault allows the south fault end to be located to within about ± 0.5 km (representing a 10% increase in model residuals from the minima).

Model Fit

Elevation changes at 94% of the BM's are satisfied within expected random and systematic errors (20 mm) by the coseismic model (Figure 4). The parameters and uncertainties (representing a 10% increase in model residuals) of the coseismic model are dip, $47° \pm 2°$, slip, 2.05 ± 0.10 m; width, 18 ± 1.7 km; and fault length, 23^{+2}_{-8} km. The model residuals are shown in Figure 6; Table 3 lists the model parameters. *Crone and Machette* [1985] measured a 1.52-m fault offset (throw) at Double Springs Pass Road on October 29, 1983, from an offset roadbed. The geodetically determined coseismic elevation change across the fault at Double Springs Pass Road was 1.56 m on November 16, 1983, and 1.58 m by June 29, 1984. The 1.5-km spacing of BM's across the fault (Z51–T10N/22E, BM's 17–18, Figure 3) limits resolution of the slip distribution in the uppermost kilometer, and so we let the model fault cut the surface.

Note the increasing tilt toward the fault on both the upthrown (BM's 1–17, Figure 4) and downthrown block (BM's 18–30). The kinks in the model at BM's 22 and 26 result from the azimuth change of the leveling route, which is shown together with the contours of elevation change predicted for the model in Figure 2*a*. The misfitting BM closest to the fault trace on the downthrown block (BM 18, a section corner) was not used in the modeling, because it does not meet the requirements for first-order survey marks and could have been unstable. Had BM 18 been retained, the best fit model would have dip of 48°, width of 18 km, length of 20 km, slip of 2.15 m, and M_0 of 2.3×10^{19} N m.

The geodetic parameters accord well with the independently measured seismic parameters. *Doser and Smith* [1985] modeled long-period body waves and obtained a focal depth of 16 ± 4 km, with the principal nodal plane dipping $45° \pm 3°$W.

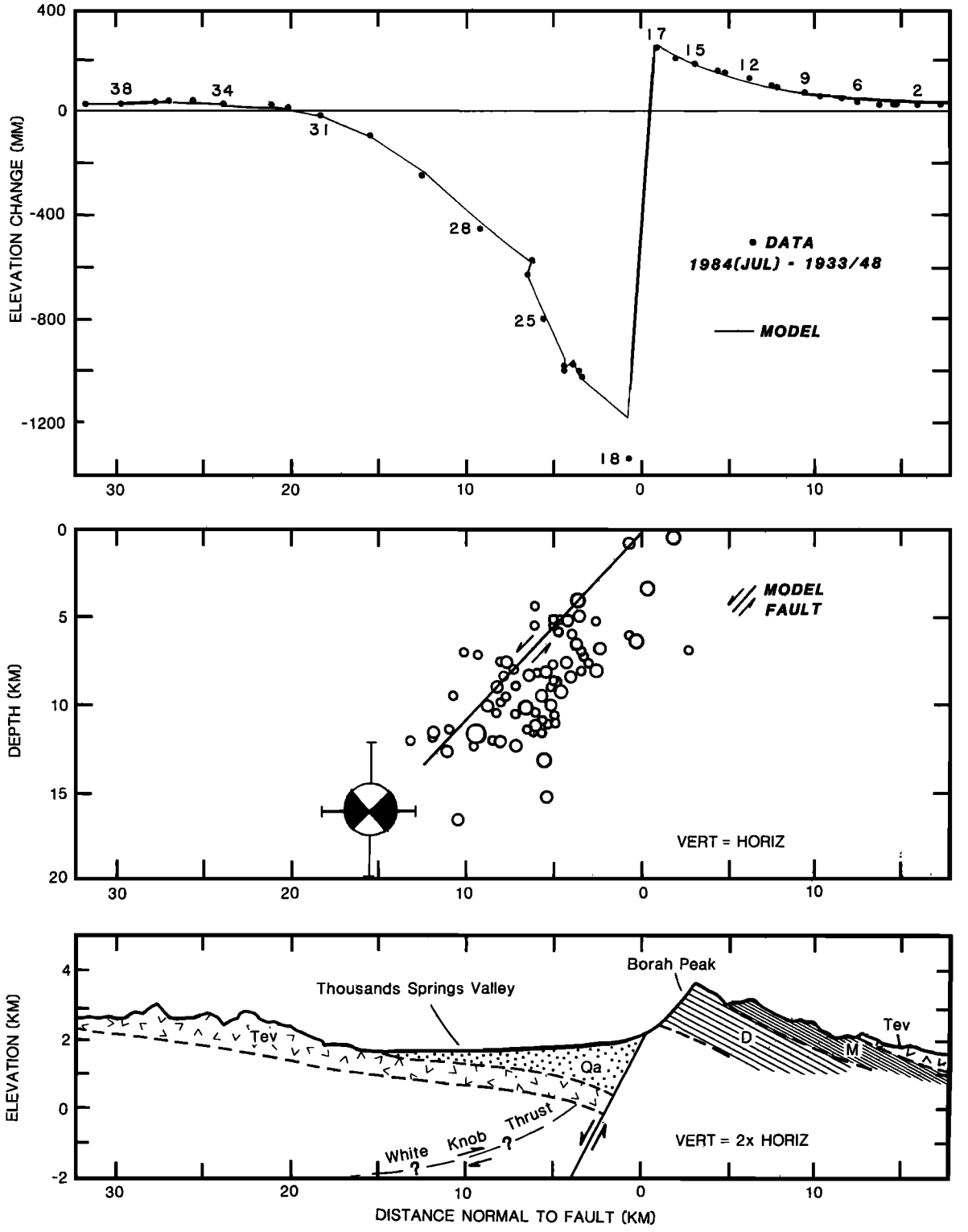

Fig. 4. (Top) Profile of observed coseismic elevation change for BM's in Figure 2*a* (dots), together with predicted changes (line) for the coseismic model. "Kinks" in the model profile result from changes in azimuth of the leveling route shown in Figure 2*a*. (Middle) Coseismic model, with main shock and aftershocks beneath the leveling line from *Richins et al.* [1985]. (Bottom) Schematic geologic cross section from *Bond* [1978]. Thickness of quaternary alluvium (Qa) is based on gravity modeling by *Mabey* [1985]. Also shown are Tertiary volcanic deposits (Tev), Mississippian (M) and Devonian (D) carbonates, and the inferred position of the White Knob thrust sheet, based on surface exposure at the northern fault end.

From the displacement spectra of teleseismic *P* waves, *Boatwright and Choy* [1985] estimate a dynamic stress drop of 2.8 MPa for the initial rupture event and a static stress drop of 1.7 MPa (17 bars) for the entire fault. Following *Kanamori and Anderson* [1975] for dip-slip faults, the static stress drop for the coseismic model is 2.9 $\pm$ 0.4 MPa (29 $\pm$ 4 bars). The geodetic moment M_0 is (2.4–3.5) $\times$ 10^{19} N m (minimum at 2.6 $\times$ 10^{19} N m), under the assumption that the shear modulus is

TABLE 3. Parameters of Basin and Range Earthquakes Deduced From Geodetic Measurements

Event	Fault					Width of Subsidence, km	Geodetic Moment M_0,* 10^{19} N m
	Dip Slip, m	Dip, deg	Length, km	Width, km	Depth, km		
1983 M = 7.0 Borah Peak†	2.05 ± 0.10	47 ± 2	23^{-2}_{+8}	18 ± 1.7	13.3 ± 1.2	15–20	$2.6^{-0.2}_{+0.9}$
1959 M = 7.3 Hebgen Lake‡	8–10	45–60	30	15	15 ± 3	20	10–14
1954 M = 7.2 Fairview Peak§	2.8	38	50	8.5	5	5	5

*The shear modulus assumed to be 3×10^4 MPa; 10^{19} N m = 10^{26} dyn cm.

†The end points of the trace of the model fault are 44°15′15″N, 113°56′04″W on the north end and 44°04′08″N, 113°48′12″W on the south end.

‡From *Savage and Hastie* [1966] and *Doser* [1985*b*].

§From *Savage and Hastie* [1969]; net slip is 4.0 m.

3×10^4 MPa (3×10^5 bars). *Barrientos et al.* [1985] find $M_0 = 1.85 \pm 0.17 \times 10^{19}$ N m by modeling the *P* and *SH* waves from synthetic seismograms, *Boatwright and Choy* [1985] found $M_0 = 1.7 \pm 0.2 \times 10^{19}$ N m, and *Doser and Smith* [1985] obtained $M_0 = 2.1 \times 10^{19}$ N m. The calculated geodetic and seismic moments are thus in substantial agreement.

Variation of Slip Along Strike

A 16-km-long segment of the leveling route that is aligned parallel to the Lost River fault (BM's 21–27, Figure 2*a*) affords a comparison of surface slip and buried fault slip. The fault throw measured by *Crone and Machette* [1984] along this segment (from Poison Spring southward to Elkhorn Creek) is shown in Figure 5 (top) together with the subsidence on the downthrown block measured from releveling (middle). The string of BM's lie 4–5 km basinward from the fault trace; the locations of the BM's and surface break are shown on the accompanying map (Figure 5, bottom). Both the subsidence and the displacement on the surface rupture decrease toward the main shock epicenter. Slip must also greatly diminish about 7–8 km northwest of the main shock, close to the south limit of surface rupture (the end of the model fault is situated at km 17 in Figure 5). This result suggests that for the Borah Peak earthquake the hypocenter is not a site of significant fault slip but rather the site where rupture initiated, with slip increasing both updip and toward the north.

INTERPRETATION

Planar Versus Listric Normal Faulting

The leveling data can be simply explained by a planar fault rupture extending from the surface to a depth of 13.3 ± 1.2 km (Figure 6). Diminished slip at a slightly greater depth is possible, because the model prescribes uniform slip everywhere on the fault. The model is consistent with analysis of the main shock and aftershocks located by *Richins et al.* [1985], plotted in Figures 4 and 6.

We examined a suite of listric faults that pass through the aftershocks and the main shock and dip 45° (listric 1) to 80° (listric 4) at the surface (Figure 7, bottom), consistent with field observations of 60°–80° dips on the 1983 Borah Peak scarp face (*Crone and Machette*, 1984]. The curved fault shape was approximated by three planar segments. The fault slip and the absolute elevation change were estimated simultaneously by least squares minimization of the residuals. The model residual for these faults are shown in Figure 7 (middle). Listric 3 (short dash), the best of the faults, shows residuals 2.0 times larger than the best fit planar fault model. Next, slip was varied in each of the three segments on the faults to determine the best fit slip distribution with depth in each case. Coseismic slip confined to the deepest portions of the model faults represents detachment faulting. Under these circumstances, listric 2a provided superior (shown in Figure 6), with uniform slip to a depth of 14.3 km and essentially no slip below this depth. Nevertheless, listric 2a has a residual 1.6 times that for the simpler planar fault. We conclude that for uniform slip, a planar or nearly planar fault fits the data best. Even a negligible amount of concave upward fault shape (listric 2a) degrades the fit to the geodetic observations. Independent support for a planar fault geometry is supplied by a study of the 43 largest aftershocks by *Smith et al.* [1985], which showed no significant variation in the dip of the nodal planes with depth.

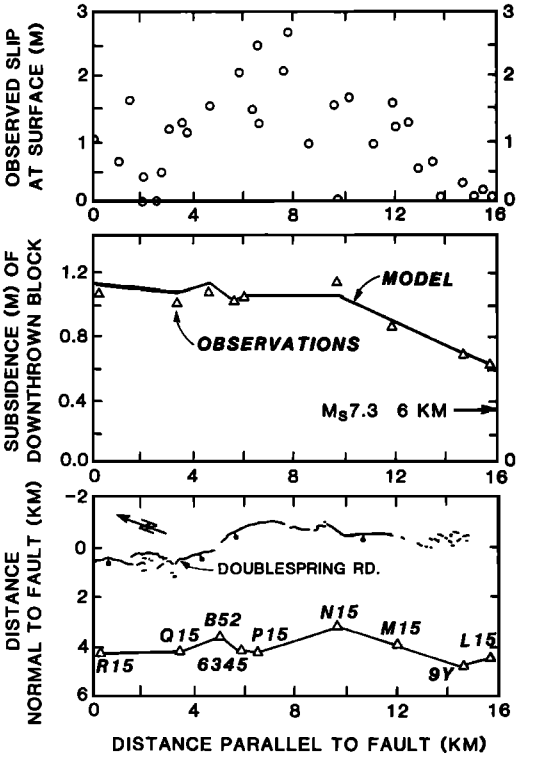

Fig. 5. Variation of surface slip and buried slip along strike. (Top) Fault throw from *Crone and Machette* [1984]. (Middle) Subsidence of the downthrown block measured by releveling, located 4–6 km from the fault trace. (Bottom) Location map for fault and BM's.

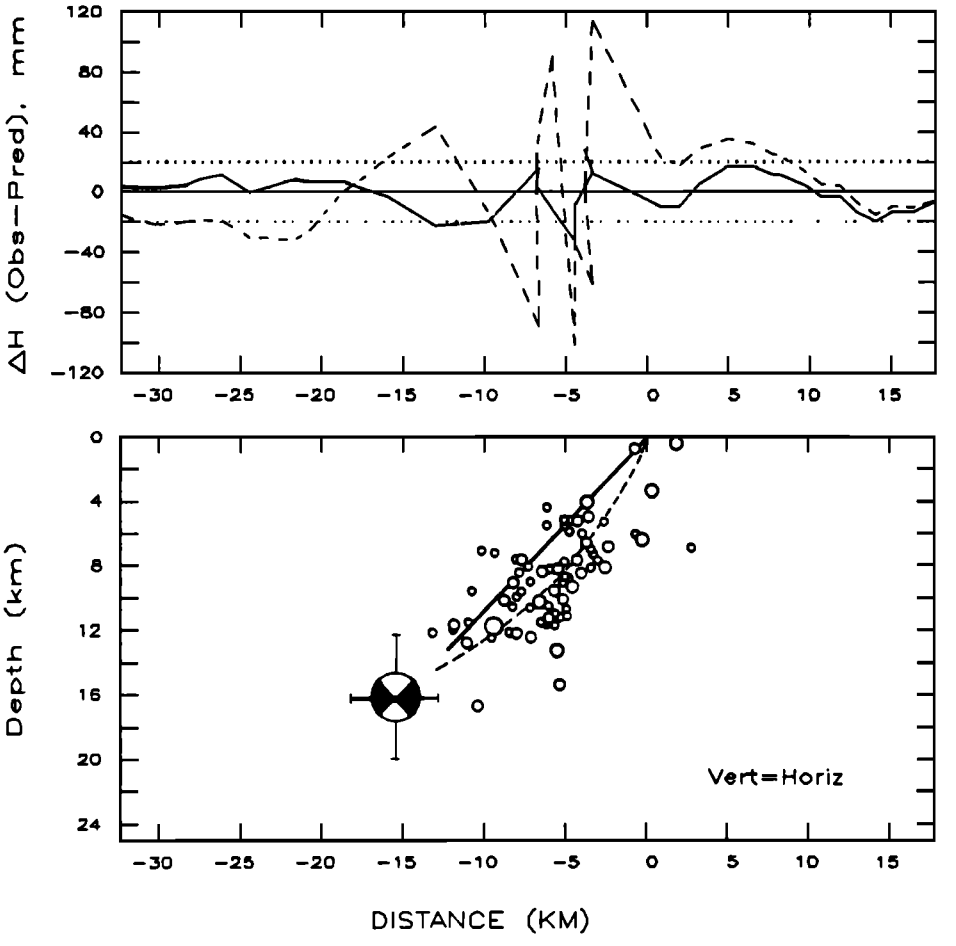

Fig. 6. (Top) Model residuals (observed − predicted elevation changes) for the best fit planar fault (solid line) and the best fit listric fault 2a (dashed line). The dotted lines enclose the 1σ observation uncertainty. (Bottom) Depth cross section of the model faults, with seismicity.

The key result of this analysis is that the Lost River fault must be nearly planar to a depth of at least 12 km. The deformation data yield no information as to the fault geometry below this depth, but they preclude any coseismic slip on low-angle or listric faults above this depth. Mesozoic thrust sheets have been proposed as the likely candidates for low-angle slip surfaces in the seismogenic crust, with the high-angle faults cut by or merging into the flat-lying faults. The White Knob thrust sheet (Figure 4) is in close proximity to the Lost River fault but did not slip and produced no aftershocks during the earthquake sequence. A number of investigators have proposed that low-angle faults are active at depth of 2–10 km [*Wernicke*, 1981; *Smith and Bruhn*, 1984; *Hamilton*, 1985]. The Borah Peak earthquake provides no support for this view, although low-angle faults may creep between earthquakes or may be active elsewhere.

The character of the deformation produced by slip on the planar high-angle fault has been previously attributed to listric fault geometries. Coseismic surface deformation steepens near the fault on both the upthrown and downthrown blocks (Figure 4); this is a dominant feature of the profiles of the data and both the planar and listric models. The pattern of increasing dip of strata toward the fault in the post-Tertiary structure (Figure 4, bottom) has been interpreted as being caused by block rotation or void accommodation resulting from a listric fault geometry [*Longwell*, 1945; *Anderson et al.*, 1983]. Increasing stratal dips toward the fault may, instead, be the product of elastic deformation associated with repeated earthquakes and thus be unrelated to block rotation.

Absolute Elevation Changes

Leveling across the Lost River Range and Thousand Springs Valley permits tentative assignment of absolute elevation changes. The end points (BM's 1 and 39, Figure 4) give the same elevation change within the measurement uncertainty (20 mm). Because the end points of the survey extend outside the region of observed and modeled coseismic deformation, they can be assumed to be fixed. Very broad wavelength tilts with magnitudes of less than 1 ppm would go undetected, however, as would uniform vertical displacement over distances greater than 50 km. Absolute uplift associated with the earthquake is 0.3 m (at BM 17); the crest of the Lost River Range in the vicinity of Borah Peak rose about 0.2 m (Figure 4). Absolute uplift of the ranges bounding a normal faulting earthquake has never before been demonstrated, because leveling was ambiguous or absent on the upthrown fault block. The maximum coseismic subsidence measured at Borah Peak was 1.2 m at the east margin of Thousand Springs Valley.

From the topographic relief, the geomorphic expression of the fault scarp, and the inferred thickness of the basin deposits, *Scott et al.* [1985] argue that 3 km of dip slip has accumulated over the past 4–7 m.y. on the Lost River fault, at a rate of 0.2–0.4 mm/yr. Repeat of events equal in size to the 1983

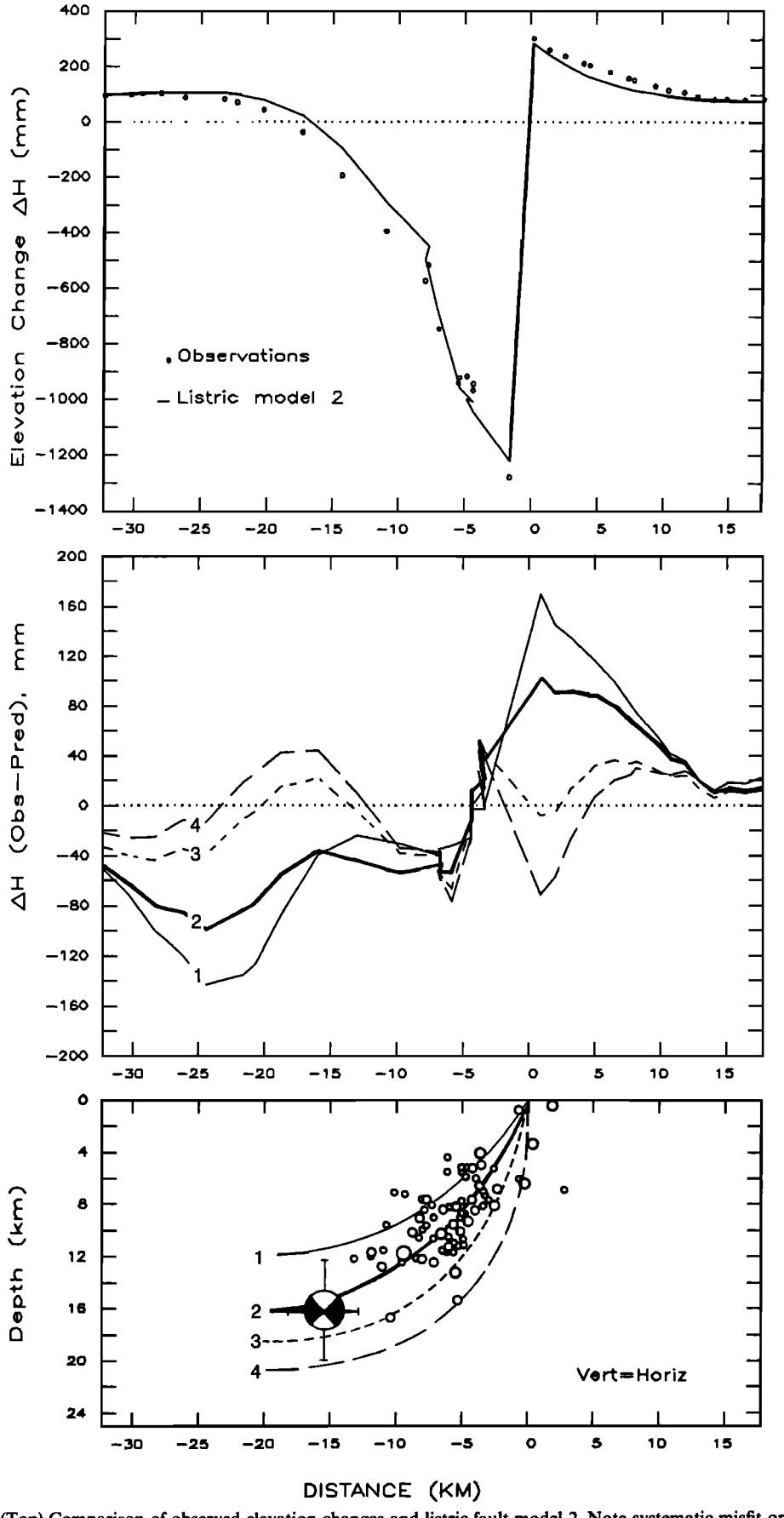

Fig. 7. (Top) Comparison of observed elevation changes and listric fault model 2. Note systematic misfit on both sides of the fault. (Middle) Residuals for four listric fault models. (Bottom) Depth cross section of the four listric fault models with seismicity.

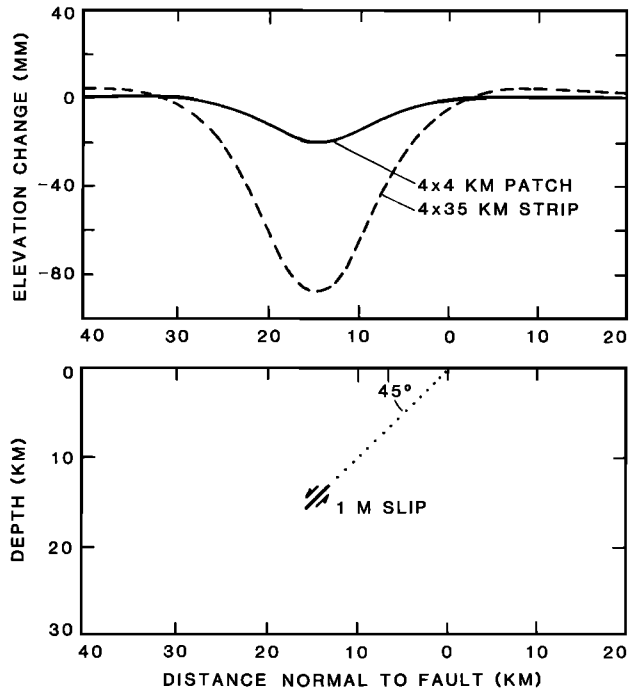

Fig. 8. Surface deformation produced by hypothetical preseismic slippage at the base of the model fault, showing elevation change per meter of fault slip caused by a 4- by 4-km epicentral patch (solid line) and a 4-km-wide strip running the 35-km length of the coseismic fault (dashed line).

shock would thus occur every 5000–10,000 years. From fault excavations near Double Springs Pass Road, *Schwartz and Crone* [1985] showed that the Lost River fault slipped about 2 m at the surface during at least one pre-1983 event in the last 12,000–14,000 years. The geodetic analysis demonstrates that the surface slip in the 1983 event closely resembles the mean slip on the fault over its entire width. Therefore it is probable that the last two events produced 4 m of cumulative slip in 14,000 years, also yielding a 0.3-mm/yr slip rate. Thus an earthquake repeat time of 5000–10,000 years is consistent with both the geologic and geodetic evidence. Unlike the coseismic displacement, however, the cumulative Pliocene displacement appears to be equally distributed between subsidence (1500 m of valley fill) and uplift (1500–2000 m of topographic relief; see Figure 4, bottom). The discrepancy between the earthquake and geologic displacements may be due to the contribution of interseismic deformation.

The coseismic deformation exhibits a strong resemblance to the structure of other basins and ranges in south central Idaho. The zones of coseismic subsidence and uplift are each about 15–20 km wide, similar to the width of Thousand Springs Valley and the Lost River Range (Figure 1). Both sides of the fault were tilted down to the east during the earthquake, a pattern of tilt consistent with the stratal dips of sedimentary rocks in the basin and the range (Figure 4) measured at the surface and inferred from a deep seismic reflection profile across Thousand Springs Valley [*Smith et al.*, 1985]. We interpret these fundamental similarities to indicate that the Borah Peak earthquake typifies the events which built the ranges.

Comparison of the Borah Peak, Fairview Peak, and Hebgen Lake Events

Although the 1954 Fairview Peak, Nevada, **M** = 7.2 event [*Savage and Hastie*, 1969; *Snay et al.*, 1985] and the 1959 Hebgen Lake, Montana, **M** = 7.3 event [*Meyers and Hamilton*, 1964; *Savage and Hastie*, 1966] may have occurred on listric faults, the seismic and available geodetic evidence favors a similar planar geometry for all three faults. The fault dips estimated from geodetic elevation changes for the events and for the Idaho shock average about 45°. *Doser* [1985*b*] found the **M** = 7.3 Hebgen Lake main shock to lie at a depth of 15 ± 3 km, with the principal nodal plane dipping 45°–60°. Table 3 lists the geodetically determined fault parameters for these three events. Neither the Nevada nor the Montana coseismic model was fitted to geodetic observations from the upthrown fault block, a circumstance that greatly hampers resolution of the fault geometry. The geodetic record for the Montana earthquake also lacks observations in the region 20–30 km from the fault on the downthrown block. The Nevada data are subject to probable systematic leveling surveying errors that have yet to be removed and that limit their utility [see *Savage and Church*, 1974, Figure 5].

The few well-studied shocks of **M** < 7 also conform to a geometry of planar faulting. The 1954 **M** = 6.8 earthquake on the Dixie Valley fault (Figure 1) also nucleated at a depth of 15 km on a fault dipping about 50°–62° [*Okaya and Thompson*, 1985; *Snay et al.*, 1985]. *Arabasz et al.* [1981] found a 13- to 14-km maximum depth of aftershocks associated with the 1975 Pocatello Valley, Idaho, **M** = 6.0 earthquake (Figure 1).

Implications for Earthquake Prediction in the Great Basin

The base of a seismic fault is a plausible site for slippage before an earthquake. Detection of preseismic fault slip at a depth of 12–15 km is a much more challenging task than if premonitory slip were to take place on a detachment surface located at much shallower depths. To monitor slip at a depth of 12–15 km on a fault dipping 45°, geodetic surveys must extend from the fault trace for about 30 km on the downthrown block, and they must have sufficient precision to detect broad-wavelength deformation. A 4- by 4-km dislocation patch situated at the base of the fault would cause the ground to subside less than 20 mm per meter of fault slip. If the zone of preseismic slippage extended 35 km along strike (for example, a 4- by 35-km strip beneath the entire Borah Peak rupture surface), then as much as 90 mm of subsidence per meter of buried slip would take place (Figure 8). For this hypothetical preseismic slip the greatest subsidence would occur within the basin, making discrimination of tectonic deformation from groundwater-related subsidence very difficult. In any case, leveling restricted to within 10 km of the fault trace will be insufficient to detect preseismic slip at the base of the fault.

CONCLUSIONS

One of the best records of coseismic elevation change ever measured for a large normal faulting event is most compatible with a planar high-angle fault rupture. The earthquake parameters deduced from geodetic observations are consistent with those gaged from seismic measurements. The 0.3 mm/yr slip rate and 5000- to 10,000-year earthquake repeat time estimated from the geodetic data and the recent geology is commensurate with geological estimates averaged over the entire 4–7 m.y. life of the Lost River fault. Absolute uplift of ranges accompanying an earthquake in a region of continental extension has been recorded.

Similarity of the fault dip (40°–50°) and the maximum depth

of fault slip (12–15 km) for the Borah Peak, Hebgen Lake, Fairview Peak, and Dixie Valley events suggests that steeply dipping planar faults pose the dominant seismic hazard in the Great Basin. The maximum depth of faulting for these events lends evidence to the hypothesis of *Sibson* [1982] and *Smith and Bruhn* [1984] that a depth of 12–15 km corresponds to the brittle-ductile transition in the crust in the Great Basin. The pattern of deformation associated with the Borah Peak earthquake, with increasing stratal dips toward the fault, has previously been interpreted as evidence for listric faulting. The existence of low-angle Mesozoic thrust sheets among the high-angle faults has given rise to the hypothesis that the relict thrust faults now undergo normal slip. Acceptance of listric faults and detachments in the upper crust as the principal sites accommodating Great Basin extension must await evidence of contemporaneous slip or Quaternary geologic displacement.

The heavily populated Wasatch fault zone in Utah shares many characteristics with the Lost River fault: Both faults show greatest cumulative surface displacement and shortest measurable repeat times near the center of the ranges, and both fault zones appear to be typified by 2-m slip events [*Schwartz and Coppersmith*, 1984; *Scott et al.*, 1985]. Whether the Wasatch fault zone also shares the subsurface geometry of the Hebgen Lake and Lost River faults is uncertain. Seismic reflection profiles across the Wasatch zone should be reexamined for deep planar bounding fault structures, as *Okaya and Thompson* [1985] have done in Dixie Valley, Nevada. Irrespective of its subsurface geometry, efforts to detect premonitory elevation change and tilt caused by slip at the base of the Wasatch fault will be demanding and require precision-leveling deformation surveys that span the fault and the downthrown block for at least 30 km, or twice the probable depth of the fault.

Acknowledgments. We are indebted to the lightning speed, skill, and tenacity of the NGS leveling crew headed by Curt Smith and guided by Bob Martine and Emery Balazs. Discussions with our colleagues at the Borah Peak Workshop and reviews by Walter Arabasz, John Langbein, Rob Reilinger, Bob Smith, Wayne Thatcher, and Mary Lou Zoback greatly improved our understanding.

REFERENCES

Allmendinger, R. W., J. W. Sharp, D. Von Tish, L. Serpa, L. Brown, S. Kaufman, and J. Oliver, Cenozoic and Mesozoic structure of the eastern Basin and Range province, Utah, from COCORP seismic-reflection data, *Geology*, *11*, 532–536, 1983.

Anderson, R. E., M. L. Zoback, and G. A. Thompson, Implications of selected subsurface data on the structural form and evolution of some basins in the northern Basin and Range province, Nevada and Utah, *Geol. Soc. Am. Bull.*, *94*, 1055–1072, 1983.

Arabasz, W. J., W. D. Richins, and C. J. Langer, The Pocatella Valley (Idaho-Utah border) earthquake sequence of March to April 1975, *Bull. Seismol. Soc. Am.*, *71*, 803–826, 1981.

Barrientos, S., S. N. Ward, J. R. González-Ruiz, and R. S. Stein, Inversion for moment as a function of depth from geodetic observations and long period body waves of the 1983 Borak Peak, ID earthquake, *U.S. Geol. Surv. Open File Rep.*, *85-290*, 485–518, 1985.

Boatwright, J., and G. L. Choy, Teleseismic estimates of the energy radiated by shallow earthquakes, *U.S. Geol. Surv. Open File Rep.*, *85-290*, 409–448, 1985.

Bomford, G., *Geodesy*, pp. 226–280, Oxford University Press, New York, 1971.

Bond, J. G., Geologic map of Idaho, Idaho Bur. of Mines and Geol., Moscow, 1978.

Crone, A. J., and S. T. Harding, Relationship of late Quaternary fault scarps to subjacent faults, eastern Great Basin, Utah, *Geology*, *12*, 292–295, 1984.

Crone, A. J., and M. N. Machette, Surface faulting accompanying the Borah Peak earthquake, central Idaho, *Geology*, *12*, 664–667, 1984.

Crosthwaite, E. G., C. A. Thomas, and K. L. Dyer, Considerations for water use and management in the Big Lost River Basin, Idaho, *U.S. Geol. Surv. Open File Rep.*, 109 pp., 1970.

Davis, G. A., Problems of intraplate extensional tectonics, western United States, in *Continental Tectonics*, pp. 84–95, National Academy of Sciences, Washington, D. C., 1980.

Doser, D. I., The 1983 Borah Peak, Idaho, and 1959 Hebgen Lake, Montana, earthquakes: Models for normal fault earthquakes in the Intermountain seismic belt, *U.S. Geol. Surv. Open File Rep.*, *85-290*, 368–384, 1985*a*.

Doser, D. I., Source parameters and faulting processes of the 1959 Hebgen Lake, Montana, earthquake sequence, *J. Geophys. Res.*, *90*, 4537–4556, 1985*b*.

Doser, D. I., and R. B. Smith, Source parameters of the 28 October 1983 Borah Peak, Idaho, earthquake from body wave analysis, *Bull. Seismol. Soc. Am.*, *75*, 1041–1051, 1985.

Eyidoğan, H., and J. Jackson, A seismological study of normal faulting in the Demirci, Alaşehir and Gediz earthquakes of 1969–1970 in western Turkey: Implications for the nature and geometry of deformation in the continental crust, *Geophys. J. R. Astron. Soc.*, *81*, 569–607, 1985.

Federal Geodetic Control Committee, *Standards and Specifications for Geodetic Control Networks*, 42 pp., National Oceanic and Atmospheric Administration, Rockville, Md., 1984.

Gilbert, G. K., A theory of earthquakes of the Great Basin, with practical application, *Am. J. Sci., 3rd Ser.*, *27*, 49–53, 1884.

Hamilton, W., Crustal extension in the Basin and Range province, southwestern United States, *J. Geol. Soc. London*, in press, 1985.

Hanks, T. C., and H. Kanamori, A moment magnitude scale, *J. Geophys. Res.*, *84*, 2348–2350, 1979.

Holdahl, S. R., A model of temperature stratification for correction of leveling refraction, *Bull. Geod.*, *55*, 231–249, 1981.

Kanamori, H., and D. L. Anderson, Theoretical basis of some empirical relations in seismology, *Bull. Seismol. Soc. Am.*, *65*, 1073–1095, 1975.

Kukkamaki, T. J., Über die nivellitische refraktion, *Publ. 25*, Finn. Geod. Inst., Helsinki, 1938.

LeConte, J., On the structure and origin of mountains, with special reference to recent objections to the "contractional theory," *Am. J. Sci.*, *26*(92), 95–112, 1878.

Longwell, C. R., Low-angle faults in the Basin and Range province, *Eos Trans. AGU*, *26*, 107–118, 1945.

Mabey, D. R., Regional gravity and magnetic anomalies in the Borah Peak region of Idaho, *U.S. Geol. Surv. Open File Rep.*, *85-290*, 680–686, 1985.

Mansinha, L., and D. E. Smylie, The displacement fields on inclined faults, *Bull. Seismol. Soc. Am.*, *61*, 1433–1440, 1971.

McTigue, D. F., and P. Segall, Vertical displacements from a dip slip fault beneath surface topography (abstract), *Eos Trans. AGU*, *65*, 1113, 1984.

McTigue, D. F., and R. S. Stein, Topographic amplification of tectonic displacement: Implications for geodetic measurement of strain changes, *J. Geophys. Res.*, *89*, 1123–1131, 1984.

Meyers, W. B., and W. Hamilton, Deformation accompanying the Hebgen Lake earthquake of August 17, 1959, *U.S. Geol. Surv. Prof. Pap.*, *435-I*, 55–98, 1964.

Nakata, J. K., C. M. Wentworth, and M. N. Machette, Quaternary fault map of the Basin and Range and Rio Grande Rift provinces, western United States, *U.S. Geol. Surv. Open File Rep.*, *82-579*, 2 sheets, 1982.

Okaya, D. A., and G. A. Thompson, Geometry of Cenozoic extensional faulting: Dixie Valley, Nevada, *Tectonics*, *4*, 107–126, 1985.

Richins, W. D., R. B. Smith, C. J. Langer, J. E. Zollweg, J. T. King, and J. C. Pechmann, The 1983 Borah Peak, Idaho, earthquake: Relationship of aftershocks to the mainshock, surface faulting, and regional tectonics, *U.S. Geol. Surv. Open File Rep.*, *85-290*, 285–310, 1985.

Savage, J. C., and J. P. Church, Evidence for postearthquake slip in the Fairview Peak, Dixie Valley, and Rainbow Mountain fault areas of Nevada, *Bull. Seismol. Soc. Am.*, *64*, 687–698, 1974.

Savage, J. C., and L. M. Hastie, Surface deformation associated with dip-slip faulting, *J. Geophys. Res.*, *71*, 4897–4904, 1966.

Savage, J. C., and L. M. Hastie, A dislocation model for the Fairview Peak, Nevada, earthquake, *Bull. Seismol. Soc. Am.*, *59*, 1937–1948, 1969.

Schwartz, D. P., and K. J. Coppersmith, Fault behavior and characteristic earthquakes: Examples from the Wasatch and San Andreas fault zones, *J. Geophys. Res.*, *89*, 5681–5698, 1984.

Schwartz, D. P., and A. J. Crone, The 1983 Borah Peak earthquake: A calibration event for quantifying earthquake recurrence and fault behavior on Great Basin normal faults, *U.S. Geol. Surv. Open File Rep., 85-290*, 153–160, 1985.

Scott, W. E., K. L. Pierce, and M. H. Hart, Jr., Quaternary tectonic setting of the 1983 Borah Peak earthquake, central Idaho, *Bull. Seismol. Soc. Am., 75*, 1053–1066, 1985.

Sibson, R. H., Fault zone models, heat flow, and the depth distribution of earthquakes in the continental crust of the United States, *Bull. Seismol. Soc. Am., 72*, 151–163, 1982.

Smith, R. B., and R. L. Bruhn, Intraplate extensional tectonics of the eastern Basin-Range: Inferences on structural style from seismic reflection data, regional tectonics, and thermal-mechanical models of brittle-ductile deformation, *J. Geophys. Res., 89*, 5733–5762, 1984.

Smith, R. B., W. D. Richins, D. I. Doser, R. K. Eddington, L. L. Leu, and G. Chen, The Borah Peak earthquake: Seismicity, faulting kinematics, and tectonic mechanism, *U. S. Geol. Surv. Open File Rep., 85-290*, 236–263, 1985.

Snay, R. A., M. W. Cline, and E. L. Timmerman, Dislocation model for the 1954 Nevada earthquakes: Preliminary report, *U.S. Geol. Surv. Open File Rep., 85-290*, 531–555, 1985.

Stearns, H. T., L. Crandall, and W. Steward, Geology and groundwater resources of the Snake River plain in southeastern Idaho, *U.S. Geol. Surv. Water Supply Pap., 774*, 260 pp., 1938.

Stein, R. S., Discrimination of tectonic displacement from slope-dependent errors in geodetic leveling from southern California, 1953–1979, in *Earthquake Prediction: An International Review, Maurice Ewing Ser.*, vol. 4, edited by D. W. Simpson and P. G. Richards, pp. 441–456, AGU, Washington, D. C., 1981.

Stein, R. S., and S. E. Barrientos, The 1983 Borah Peak, Idaho, earthquake: Geodetic evidence for deep rupture on a planar fault, *U.S. Geol. Surv. Open File Rep., 85-290*, 459–484, 1985.

Stewart, J. H., Basin and Range structure: A system of horsts and grabens produced by deep-seated extension, *Geol. Soc. Am. Bull., 82*, 1019–1044, 1971.

Wallace, R. E., Patterns and timing of late Quaternary faulting in the Great Basin province and relation to some regional tectonic features, *J. Geophys Res., 89*, 5763–5769, 1984*a*.

Wallace, R. E., Fault scarps formed during the earthquake of October 2, 1915, in Pleasant Valley, Nevada, and some tectonic implications, *U.S. Geol. Surv. Prof. Pap., 1274-A*, 33 pp., 1984*b*.

Wernicke, B., Low-angle normal faults in the Basin and Range province: Nappe tectonics in an extending orogen, *Nature, 291*, 645–648, 1981.

Whalen, C. T., and E. Balazs, Test results of first-order class III leveling, *NOAA Tech. Rep., NOS 68 NGS 4*, 30 pp., 1977.

Whitehead, R. L., R. W. Harper, and H. G. Sisco, Hydrologic changes associated with the October 28, 1983, Idaho earthquake, *Pure Appl. Geophys., 122*, 280–293, 1984.

S. E. Barrientos, C. F. Richter Laboratory, University of California, Santa Cruz, CA 95046.

R. S. Stein, U.S. Geological Survey, 345 Middlefield Road, MS/977, Menlo Park, CA 94025.

(Received January 16, 1985;
revised July 1, 1985;
accepted July 2, 1985.)